IEEE Access
Multidisciplinary ⋮ Rapid Review ⋮ Open Access Journal

Received June 8, 2021, accepted June 11, 2021, date of publication June 15, 2021, date of current version June 24, 2021.

Digital Object Identifier 10.1109/ACCESS.2021.3089465

High Efficiency Electro-Optic Modulation in a Graphene Silicon Hybrid Tapered Microring Resonator

YONGHUA WANG[1,2,3], LEI LEI[1,3], JUNBIN ZANG[4], WENCHAN DONG[5,6], XINLIANG ZHANG[5,6], (Senior Member, IEEE), AND PING XU[1,3]

[1]College of Physics and Optoelectronic Engineering, Shenzhen University, Shenzhen 518060, China
[2]College of Electrical Engineering, North China University of Science and Technology, Tangshan 063210, China
[3]Key Laboratory of Optoelectronic Devices and Systems of Ministry of Education and Guangdong Province, Shenzhen 518060, China
[4]Science and Technology on Electronic Test and Measurement Laboratory, North University of China, Taiyuan 030051, China
[5]Wuhan National Laboratory for Optoelectronics, Huazhong University of Science and Technology, Wuhan 430074, China
[6]School of Optical and Electronic Information, Huazhong University of Science and Technology, Wuhan 430074, China

Corresponding authors: Lei Lei (leilei@szu.edu.cn) and Wenchan Dong (wcdong@hust.edu.cn)

This work was supported in part by the National Key Research and Development Program of China under Grant 2019YFB2203102, in part by the National Natural Science Foundation of China (NSFC) under Grant 61805151, in part by the Natural Science Foundation of Hebei Province under Grant F2019209599, in part by the China Postdoctoral Science Foundation under Grant 2020M672783, and in part by the Key Technologies Research and Development Program of Shenzhen under Grant JSGG20201102173200001.

ABSTRACT Graphene silicon devices have attracted significant attention due to their outstanding electronic and optical properties. By electrically tuning the Fermi level of the monolayer graphene sheet, electro-optic (EO) modulators have been widely analyzed. Despite significant progress has been achieved on high-speed modulation with integrated graphene silicon waveguides, it remains challenging to realize a high modulation efficiency since the light absorption in graphene is limited. Here, we propose and experimentally demonstrate a high efficiency EO modulator using a graphene-assisted tapered silicon ring resonator, where the tapered zone is covered by a graphene/graphene capacitor. This graphene-assisted tapered zone strongly enhances the graphene-light interaction that the achieved static and dynamic modulation (1KHz) depths are up to 26 dB and 12 dB, respectively. Physical mechanism of the modulation based on this nanostructure is also discussed in detail. The proposed nanostructure provides a promising alternative method for high-performance EO modulator, which is essential for the on-chip optical communication, optical computing and optical signal processing.

INDEX TERMS Graphene photonics, silicon microring resonators, electro-optic modulation.

I. INTRODUCTION

Graphene, a two-dimensional version of graphite that consists of a single layer of carbon atoms, has attracted a significant research attention because of its exceptional properties including high carrier mobility [1], large broadband absorption [2], [3], zero-band gap, and tunable Fermi level [4]–[6]. In particular, the remarkable optical properties [7] have made graphene a promising material for high-performance electro-optical (EO) devices such as fast and broadband photodetector and modulator [8]–[23]. The wavelength-independent interband absorption in graphene can be blocked by Pauli blocking when $|E_F| > \hbar\omega/2$, where E_F is the Fermi energy and $\hbar\omega$ is the photon energy. A notable consequence of the low density state is that the charge-carrier density can change, which accordingly makes the Fermi level shifting available by applying a gate voltage to the graphene [20]. This electrically tunable Fermi level leads to a synchronous light absorption, enabling the ultra wideband electric-optic modulation in the graphene silicon hybrid nanophotonic integrated circuits. [10]–[13].

To achieve a highly efficient modulation of the graphene optical modulator, it is very important to enhance the interaction between the light and graphene monolayer. One way to improve the interaction is increasing the effective interaction length between the coupled evanescent wave and the

The associate editor coordinating the review of this manuscript and approving it for publication was Sukhdev Roy.

graphene [10]–[12]. However, due to the high refractive index of silicon, the optical field is mainly confined within the waveguide and has limited interaction with the graphene layer. As a result, the graphene-light interaction might be too low to obtain a deep modulation depth. In order to enhance the modulation depth, the silicon waveguide is then replaced by a silicon ring resonator [13], [20], whose resonance is more sensitive to graphene than that of a traditional straight waveguide. Another similar attractive alternative is to use the slot waveguide [24]. The slot dramatically enhances the graphene-light interaction while simultaneously induces high loss, which is of paramount importance for the modulator setup. These methods effectively improve the modulation depth, but still suffer from the unexpected nonlinearity and limited carrier mobility associated with the doped silicon back gate.

In this work, we propose and experimentally demonstrate an enhanced graphene-light interaction mechanism in a graphene-assisted irregular ring resonator for high efficiency EO modulation. Specifically, the configuration of the proposed nanostructure consists of a tapered silicon ring resonator, of which the tapered zone is covered by a graphene/graphene capacitor. In this structure, the graphene-light interaction is not only enhanced by the ring resonator that improves the absorption, but also by the tapered segment under the graphene, which is mainly in charge of strengthening the graphene-light interaction and correspondingly realizes the high modulation depth. A proof of principle for the modulation is carried out by an electric gate signal with an amplitude of 5V at the frequency of 1kHz. An ultra-high modulation depth of 26 dB is achieved as the bias voltage is 8V. Our structural design and experimental demonstration show that graphene EO modulator has the potential not only for high speed modulation but also for high depth modulation.

II. DEVICE DESIGN

The common method of enhancing the interband absorption of graphene is to enlarge the graphene coverage on the ring resonator. However, this increased interaction area simultaneously induces a higher contact resistance as well as the capacitance of the graphene/graphene capacitor. Also, it reduces the quality factor (Q) of the resonator due to defects in the large graphene coverage. All these reasons make it challenging to further improve the modulation depth, which is one of the most important features for a modulator. Our proposal of the graphene-assisted silicon tapered ring resonator is depicted in Fig. 1(a). Compared to the conventional structure, the width of the ring covered by the graphene in our device is gradually changed. Specifically, it is much narrower in the middle while wider at both ends that we call it the tapered segment of the ring, and the narrowest position is named as a waist. To investigate the light absorption enhancement of the proposed nanostructure, the normalized electric field distributions of TE mode with different waist widths are shown in Fig. 1(b). It is seen that with a narrower waist, more energy leaks from the waveguide and interacts with the

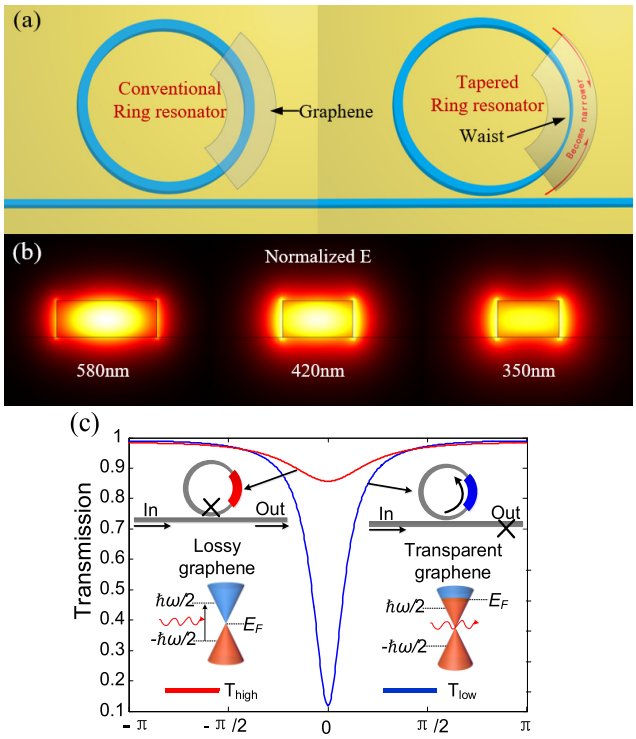

FIGURE 1. (a) Schematic diagrams of the conventional graphene-silicon hybrid ring resonator and the proposed tapered nanostructure. (b) The TE mode field profiles of the ring waist with different widths. (c) Modulation mechanism of the graphene-ring resonator.

graphene. This enhanced light-graphene interaction indeed promises the strong absorption in the graphene to fulfill the amplitude modulation.

Fig. 1(c) shows the modulation mechanism of the graphene-ring resonator. The relationship between charge-carrier density n in graphene and the applied voltage V can be expressed as $n = (V + V_0)\varepsilon_0\varepsilon/t_g e$, where V_0 is the voltage offset induced from the natural doping, ε_0 and ε denote the permittivities of the free space and dielectric spacer of the graphene capacitor, respectively. t_g refers to the thickness of the dielectric layer, and e is the electron charge. The Fermi level of graphene shifts according to $E_F = \hbar v_F(\pi|n|)^{1/2}$ [6], where $\hbar$ is the Planck's constant divided by 2π and v_F is the Fermi velocity. When the bias voltage, which is dependent on the Fermi level E_F, is close to the Dirac point, interband absorption occurs as the electrons are excited by the incident photons ($\hbar\omega$). As a result, the graphene layers become highly lossy and the transmission of the graphene-assisted tapered ring resonator exhibits a high transmission as shown in the red line (T_{high}). On the contrary, when E_F is greater than half the photon energy of the incident light (i.e., $|E_F| > \hbar\omega/2$), all the electron states in the graphene would be filled and no interband transition is allowed due to Pauli blocking. In this condition, the graphene layers turn to be transparent, leading to an intensive resonance as shown in the blue line (T_{low}). The round-trip loss of the underlying ring waveguide changes significantly as the absorption of the graphene layers change.

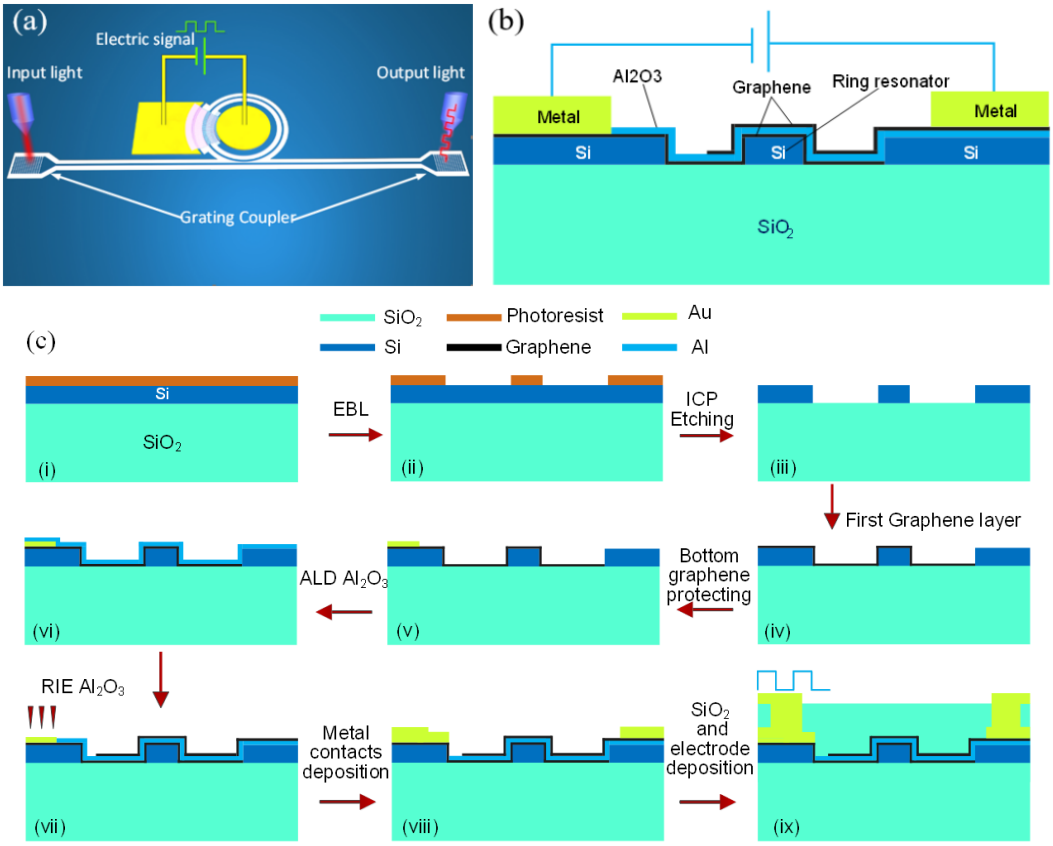

FIGURE 2. **(a) Configuration of the proposed graphene silicon hybrid EO modulator. (b) Cross-section of the ring resonator covered with the graphene/graphene capacitor. (c) Detailed fabrication process flow diagram.**

The loss of the ring ultimately influences the resonance depth, and the transmission difference between the high and low loss resonances is regarded as the modulation depth.

In this work, the resonator is designed for critical coupling at T_{low} state (high bias) and under coupling at T_{high} state (0 V bias). There is another option of designing for critical coupling at T_{low} state (0 V bias) while over coupling state at T_{high} (high bias) [14]. Both of these two approaches can be used for the high depth modulation.

III. DEVICE FABRICATION

The modulation process is depicted in Fig. 2(a). An optical continuous wave (CW) is coupled into the device by the input grating coupler and coupled into the ring. The CW light is then modulated by an electric gate signal added the graphene through the metal electrodes. The cross-section of this functional module is shown in Fig. 2(b). Here, the graphene layer is placed on the top of the tapered zone and consists of two monolayer graphenes separated by an oxide spacer. This sandwich structure makes up a parallel capacitor to avoid using the doped silicon back gate. When applying the electric drive signal, the two graphene layers are doped to the same level, one with holes while the other with electrons. The Fermi energy (E_F) then exhibits a significant shift, which in turn alters the rate of the interband transition and realizes the light modulation. Eventually, an optical amplitude modulated signal synchronous with the drive signal can be achieved at the output grating coupler of the device.

The fabrication process flow diagram is shown in Fig. 2(c). The device is fabricated on standard SOI wafers with the silicon thickness of 220 nm and buried-oxide thickness of 3 μm. For the ring resonator, the radius is 20 μm and the gap between the ring and the bus waveguide is 100 nm. The normal zone as well as the bus waveguide and waist of the ring are wide as 500 nm and 350 nm, respectively. The pattern of the device is then transferred to the silicon layer through the electron beam lithography (EBL) and inductively coupled plasma (ICP) etching ((i)-(iii)). with the fully etched depth of 220 nm. It is noted that before transferring the underlying graphene layer, a 5 nm Al_2O_3 is directly deposited by atomic layer deposition (ALD), which is not shown in Fig. 2(c), to prevent the potential carrier injection into the silicon from the underlying graphene layer. The bottom graphene monolayer of the graphene/graphene capacitor is then grown by the chemical vapor deposition (CVD) on copper foil and wet-transferred onto the adhesion layer of Al_2O_3 (iv). This fabrication process is consistent with our previous work on EIT-like phenomenon [25]. On the bottom graphene, a layer of Ti/Au with the respective thickness of 10 nm and 50 nm is deposited using the electron-beam evaporation and then

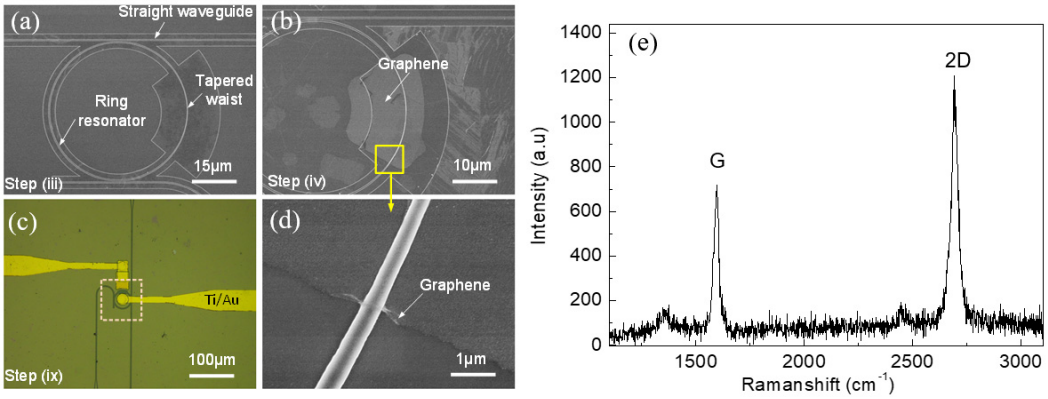

FIGURE 3. (a)-(d) SEM and optical microscopy images of the fabricated device with the related fabrication steps labeled in Fig. 2(c). (e) Raman spectrum of the monolayer graphene sheet.

patterned by the lift-off process (v). This step well protects the bottom graphene from the electric contacting during the etching of Al_2O_3 spacer.

Since graphene is intrinsically hydrophobic, it is very challenging to deposit the Al_2O_3 spacer directly on the graphene. Thus, we firstly depose 1 nm layer of aluminum using electron-beam evaporation and immediately oxidize it into Al_2O_3 in the ambient air. The generated 1 nm Al_2O_3 can be regarded as the seed layer of the following 19 nm Al_2O_3 deposition by ALD [11], indicating the total thickness of the Al_2O_3 spacer is 20 nm. The thickness of 20 nm not only ensures the quality of the dielectric spacer, but also makes it easier to measure the thickness based on our fabrication condition. The top graphene is then wet-transferred to the Al_2O_3 spacer as discussed before (vi). Reactive ion etching (RIE) is subsequently followed on the graphene/graphene capacitor for contacting the electrode and the bottom graphene (vii). Two Ti/Au (10/100nm) electrodes are added to each graphene layer by electron-beam evaporation (viii) for the electric driving. Finally, to avoid the loss induced by the metal electrodes, we deposit a SiO_2 cladding on top of the nanostructure with the thickness of 1 μm by plasma-enhanced CVD (ix).

The scanning electron microscopy (SEM) and optical microscopy images of the proposed device are shown in Fig. 3(a)–Fig. 3(d) with the related fabrication steps labeled in Fig. 2(c). Thanks to the high strength of the graphene caused by its honeycomb structure, one can see that the graphene layer is well covered on the ring. Fig. 3(e) illustrates the measured Raman spectrum of the transferred graphene sheet. The G and 2D peaks present at 1590 cm^{-1} and 2683 cm^{-1}, respectively, indicating that the graphene monolayer is of good quality.

IV. DEVICE PERFORMANCE

In the experiment, a CW light is generated from a tunable laser (New Focus TLB-6728-P) with the average power of 13 dBm. Followed by the polarization beam splitting and the polarization optimizing, the light is then injected into the grating coupler through a 75° lensed fiber that is aligned with a precision translation stage (New Focus M-461-XYZ-M). The average power at the output of the polarization controller is measured about 7dBm. The grating couplers show the loss of 5dB for each port. The transmission spectra are measured by sweeping the wavelength of the laser and observed via the digital spectrum analyzer (Tektronix MDO3054) with a photo detection (New Focus 1811).

As a comparison, the measurement of a conventional ring resonator is also shown here. The geometry of the referenced ring resonator is identical to that of the proposed tapered one except that the width of the ring remains constant. Fig. 4(a) and 4(b) compare the transmission spectra of the conventional and tapered ring resonators without graphene. In this case, the transmission minimum on resonance (TMR) of tapered ring resonator is −46 dB, slightly smaller than that of the conventional one whose TMR is measured as −51 dB. The quality factor (Q) also slightly decreases from 22000 to 17000 compared to the regular and tapered nanostructures. The performance degradation in TMR and Q can be attributed to the radiation loss in the tapered zone of the proposed resonator. After adding the graphene layers, the TMR of the conventional ring resonator is reduced to −23.5 dB as shown in Fig. 4(c). While in Fig. 4(d), the TMR of the tapered one is further reduced to −12.8 dB due to the strong graphene-light interactions in the narrow part of the ring. Since there is no applied voltage, the Fermi level of the graphene is so close to the Dirac point that the interband absorption is very strong. These results show that the graphene-assisted tapered ring exhibits a more intensive absorption of the transmitting light, allowing the capability of a deep modulation depth.

The electro-optic modulation performance of the device is investigated by applying different bias voltages to the graphene/graphene capacitor. At zero bias, the Fermi level of the graphene is close to the Dirac point and the interband absorption is very strong. This is associated with the electrons in the graphene excited by the photons in the evanescent field of the ring. Correspondingly, the ring shows a high loss that the whole resonator works under the under coupling state.

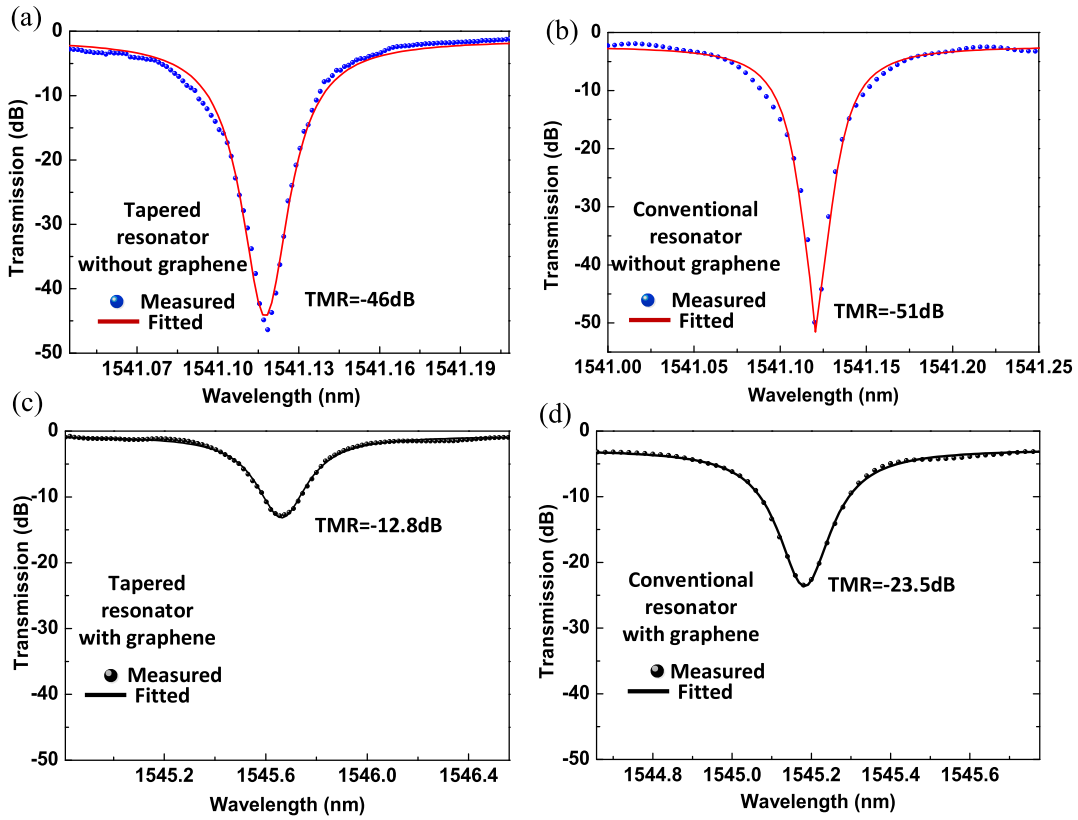

FIGURE 4. Measured transmission spectra (dots) and Lorentz fitting curves (lines). (a) The conventional ring resonator without graphene. (b) The tapered ring resonator without graphene. (c) The conventional ring resonator with graphene. (d) The tapered ring resonator with graphene.

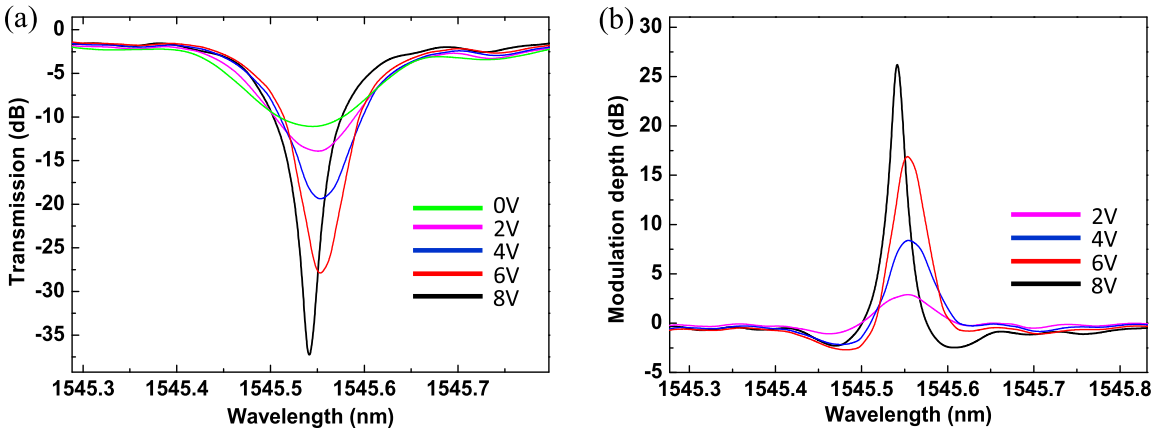

FIGURE 5. (a) Measured transmission spectra of the tapered resonator covered with the graphene/graphene capacitor at different bias voltages. (b) Measured modulation depth with different bias voltages.

Thus, without the bias, TMR of the proposed EO modulator is measured just as −11dB as shown in the green line in Fig. 5(a). By increasing the bias voltage, the doping level goes heavier which blocks the graphene optical absorption and leads to a lower loss. The TMR of −37dB is obtained at the bias of 8V as shown in the dark line in Fig. 5(a). It is worth noting that the TMR does not keep rising as the bias voltage further increases. This is because that as the bias is higher than 8V, the Fermi level is going to be far away from the Dirac point and the loss induced by the graphene will reach to a minimum due to the Pauli blocking. Additionally, according to Fig. 5(a), the insertion loss, which is defined as the lower insertion loss between before and after the graphene tuning, is measured as 11dB. The evolution of modulation depth illustrated in Fig. 5(b) matches well with TMR. Specifically, the higher TMR enables the deeper modulation depth. It is

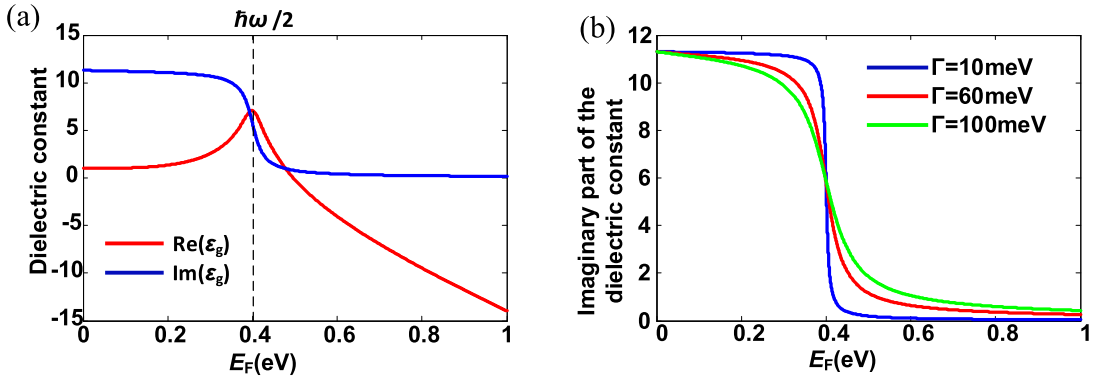

FIGURE 6. (a) Evolution in the real and imaginary parts of the dielectric constant depending on the Fermi level. (b) Impact of the interband transition broadening Γ on the imaginary part of the dielectric constant.

seen that the optimal modulation depth is measured as high as 26 dB. Meanwhile, the resonance shows a blue shift as the voltage increases. This shift could be attributed to the real part of the dielectric constant (ε_g') of graphene which changes with the voltage-dependent Fermi level and is similar to the resonance frequency shifts observed in graphene with optical plasmon resonance [26], as we describe below.

To be more specific, as expressed in Eq. (1) and (2), the real (ε_g') and imaginary (ε_g'') parts of the complex dielectric constant (ε_g) of graphene are related to its optical conductivity σ and a complex form of the Kubo formula that involves the interband and intraband contributions [27]–[29].

$$\varepsilon_g' = 1 + \frac{e^2}{8\pi\hbar\omega\varepsilon_0 t_g}\ln\frac{(\hbar\omega+2|E_F|)^2+(2\pi\hbar/\tau_2)^2}{(\hbar\omega-2|E_F|)^2+(2\pi\hbar/\tau_2)^2} - \frac{e^2|E_F|}{\pi\varepsilon_0 t_g\left[(\hbar\omega)^2+(2\pi\hbar/\tau_1)^2\right]} \tag{1}$$

$$\varepsilon_g'' = \frac{e^2}{4\hbar\omega\varepsilon_0 t_g} \times\left[1+\frac{1}{\pi}\left(\tan^{-1}\frac{\hbar\omega-2|E_F|}{2\pi\hbar/\tau_2}-\tan^{-1}\frac{\hbar\omega+2|E_F|}{2\pi\hbar/\tau_2}\right)\right] + \frac{2e^2|E_F|}{\omega\tau_1\varepsilon_0 t_g\left[(\hbar\omega)^2+(2\pi\hbar/\tau_1)^2\right]} \tag{2}$$

In the equations, the photon energy $\hbar\omega$ of the incident light is set as 0.8 eV at the wavelength of 1545 nm. τ_1 is the relaxation time associated with carrier-carrier intraband collision and phonon emission. τ_2 denotes the relaxation time associated with the electron interband relaxation and cooling of hot phonons [30]–[34]. Since the former relaxation time τ_1 is usually estimated as hundreds of femtoseconds [29], the term $2\pi\hbar/\tau_1$ in Eq. (1) and (2) can be totally neglected. Conversely, the latter one τ_2 needs to be well taken into account cause it has been measured at the level of picoseconds [32], [33]. Here, we set $\Gamma = 2\pi\hbar/\tau_2$, thus Γ can be regarded as the interband transition broadening [13].

The imaginary part of dielectric constant ε_g'' is characterized by interband and intraband absorption [26]. As a consequence, ε_g'' has a step-like falling at the Fermi level threshold $E_F = \hbar\omega/2$, as shown in Fig. 6(a) (blue line). Ideally, when the Fermi level is higher than the threshold $E_F = \hbar\omega/2$ or lower than $E_F = -\hbar\omega/2$, the loss in the ring should have changed suddenly. However, from Fig. 5(a), it is found that the measured transmission spectrum gradually changes with the increasing bias voltage. This can be explained by the fact that ε_g'' is closely related to Γ. As displayed in Fig. 6(b), the Γ is higher, the ε_g'' goes smoother. Since Γ has been estimated larger than 100 meV [13], [26], the transmission spectrum shows a gradual change. Similarly, the real part of the index $\mathrm{Re}(n_{eff})$ affects the resonance shift and so does the ε_g'. As a result, the red and blue shifts of the transparency peak displayed in Fig. 5 can be well explained by the characteristics of ε_g' shown in Fig. 6a (red line). One can see that the ε_g' peaks at the Fermi level of $\hbar\omega/2$, while it declines either the E_F gets higher or lower. Accordingly, this "$\hbar\omega/2$" cut-off performs as the division of the red and blue shifts of the resonance.

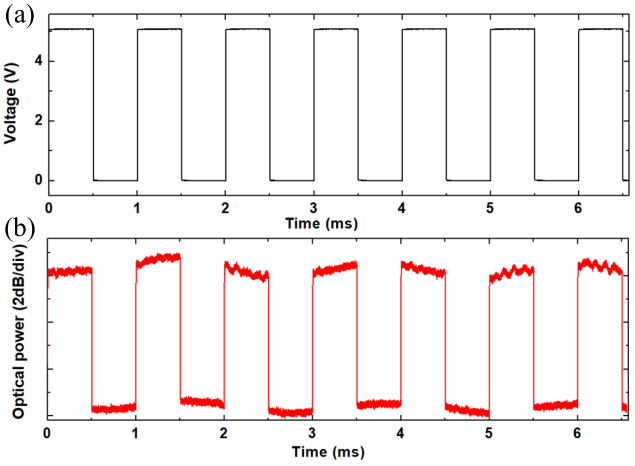

FIGURE 7. Amplitude modulation performance of the proposed graphene silicon hybrid tapered ring resonator. (a) Electrical drive square signal with the peak-to-peak amplitude of 5V. (b) Modulated optical signal with the extinction ratio of 12 dB.

The EO modulation performance of the proposed graphene silicon hybrid tapered ring resonator is tested via a proof-of-concept experiment with a $5V_{pp}$ square waveform as shown in Fig. 7(a). A CW light at 1545.55 nm is launched into

the modulator with an average power of 13dBm. The measured modulated optical signal is illustrated in Fig. 7(b). It is observed that the modulated optical signal exhibits a good on-off switching performance without any broadening at the edges, which is benefit from the high modulation efficiency and modulation depth of the modulator. The measured extinction ratio of the modulated signal is up to 12 dB. Note that it is also possible to reduce the bias voltage while maintain the modulation depth. In this case, dielectric material with a higher permittivity would be expected to work as the spacer or the thickness of the Al_2O_3 spacer should be decreased with improved deposition. The lower working voltage enables the potential to drive the EO modulator directly from the CMOS output without any driver. The modulation bandwidth of the proposed device is comparatively limited here due to the growing resistance and capacitance associated with the accumulated fabrication defects. By further simplifying the fabrication steps and optimizing the fabrication conditions, the modulation bandwidth over tens of GHz can be expected [35].

V. CONCLUSION

In conclusion, we have experimentally realized a high efficiency amplitude modulation in a graphene silicon hybrid tapered ring resonator. The tapered zone assisted by the graphene/graphene capacitor intensively enhances the graphene-light interaction, which plays an important role in improving the modulation depth. The Fermi level, tuned by increasing the bias voltage, greatly affects the dielectric constant of the graphene. Based on this mechanism, both the resonance shift and evolution of the modulation depth, affected by increasing the bias voltage are well discussed and explained. The performance of the proposed modulator is demonstrated by a proof-of-concept experiment. We achieve an ultrahigh modulation depth of 26 dB with the bias voltage of 8V. The modulated optical signal exhibits a good on-off switching performance with steep edges and the measured extinction ratio is up to 12dB, which is benefit from the high modulation efficiency and modulation depth of the modulator. The proposed nanostructure offers a way for high-performance EO modulation applied in integrated photonics, nonlinear optics, visible photonics and so on.

REFERENCES

[1] K. I. Bolotin, K. J. Sikes, Z. Jiang, M. Klima, G. Fudenberg, J. Hone, P. Kim, and H. L. Stormer, "Ultrahigh electron mobility in suspended graphene," *Solid State Commun.*, vol. 146, nos. 9–10, pp. 351–355, Jun. 2008.

[2] Q. Bao, H. Zhang, B. Wang, Z. Ni, C. H. Y. X. Lim, Y. Wang, D. Y. Tang, and K. P. Loh, "Broadband graphene polarizer," *Nature Photon.*, vol. 5, no. 7, pp. 411–415, May 2011.

[3] K. F. Mak, M. Y. Sfeir, Y. Wu, C. H. Lui, J. A. Misewich, and T. F. Heinz, "Measurement of the optical conductivity of graphene," *Phys. Rev. Lett.*, vol. 101, no. 19, Nov. 2008, Art. no. 411196405.

[4] K. S. Novoselov, A. K. Geim, S. V. Morozov, D. Jiang, Y. Zhang, S. V. Dubonos, I. V. Grigorieva, and A. A. Firsov, "Electric field effect in atomically thin carbon films," *Science*, vol. 306, no. 5696, pp. 666–669, Oct. 2004.

[5] A. K. Geim and K. S. Novoselov, "The rise of graphene," *Nature Mater.*, vol. 6, no. 3, pp. 183–191, Mar. 2007.

[6] F. Wang, Y. Zhang, C. Tian, C. Girit, A. Zettl, M. Crommie, and Y. R. Shen, "Gate-variable optical transitions in graphene," *Science*, vol. 320, no. 5873, pp. 206–209, Apr. 2008.

[7] F. Bonaccorso, Z. Sun, T. Hasan, and A. C. Ferrari, "Graphene photonics and optoelectronics," *Nature Photon.*, vol. 4, no. 9, pp. 611–622, Aug. 2010.

[8] A. Pospischil, M. Humer, M. M. Furchi, D. Bachmann, R. Guider, T. Fromherz, and T. Mueller, "CMOS-compatible graphene photodetector covering all optical communication bands," *Nature Photon.*, vol. 7, no. 11, pp. 892–896, Sep. 2013.

[9] M. Furchi, A. Urich, A. Pospischil, G. Lilley, K. Unterrainer, H. Detz, P. Klang, A. M. Andrews, W. Schrenk, G. Strasser, and T. Mueller, "Microcavity-integrated graphene photodetector," *Nano Lett.*, vol. 12, no. 6, pp. 2773–2777, May 2012.

[10] M. Liu, X. Yin, E. Ulin-Avila, B. Geng, T. Zentgraf, L. Ju, F. Wang, and X. Zhang, "A graphene-based broadband optical modulator," *Nature*, vol. 474, no. 7349, pp. 64–67, May 2011.

[11] M. Liu, X. Yin, and X. Zhang, "Double-layer graphene optical modulator," *Nano Lett.*, vol. 12, no. 3, pp. 1482–1485, Feb. 2012.

[12] Y. Hu, M. Pantouvaki, J. Van Campenhout, S. Brems, I. Asselberghs, C. Huyghebaert, P. Absil, and D. Van Thourhout, "Broadband 10 Gb/s operation of graphene electro-absorption modulator on silicon," *Laser Photon. Rev.*, vol. 10, no. 2, pp. 307–316, Jan. 2016.

[13] C. Qiu, W. Gao, R. Vajtai, P. M. Ajayan, J. Kono, and Q. Xu, "Efficient modulation of 1.55 μm radiation with gated graphene on a silicon microring resonator," *Nano Lett.*, vol. 14, no. 12, pp. 6811–6815, Nov. 2014.

[14] G. Sinatkas, T. Christopoulos, O. Tsilipakos, and E. E. Kriezis, "Comparative study of silicon photonic modulators based on transparent conducting oxide and graphene," *Phys. Rev. A, Gen. Phys.*, vol. 12, no. 6, Dec. 2019, Art. no. 064023.

[15] T. Christopoulos, O. Tsilipakos, G. Sinatkas, and E. E. Kriezis, "On the calculation of the quality factor in contemporary photonic resonant structures," *Opt. Exp.*, vol. 27, no. 10, pp. 14505–14522, Apr. 2019.

[16] A. Pitilakis, D. Chatzidimitriou, and E. E. Kriezis, "Theoretical and numerical modeling of linear and nonlinear propagation in graphene waveguides," *Opt. Quantum Electron.*, vol. 48, no. 4, Mar. 2016, Art. no. 243.

[17] K. Alexander, N. A. Savostianova, S. A. Mikhailov, D. Van Thourhout, and B. Kuyken, "Gate-tunable nonlinear refraction and absorption in graphene-covered silicon nitride waveguides," *ACS Photon.*, vol. 5, no. 12, pp. 4944–4950, Nov. 2018.

[18] Y. Ding, X. Guan, X. Zhu, H. Hu, S. I. Bozhevolnyi, L. K. Oxenløwe, K. J. Jin, N. A. Mortensen, and S. Xiao, "Efficient electro-optic modulation in low-loss graphene-plasmonic slot waveguides," *Nanoscale*, vol. 9, no. 40, pp. 15576–15581, 2017.

[19] C. Zhong, J. Li, and H. Lin, "Graphene based all-optical modulators," *Frontiers Optoelectron.*, vol. 13, no. 2, pp. 114–128, Jun. 2020.

[20] Y. Ding, X. Zhu, S. Xiao, H. Hu, L. H. Frandsen, N. A. Mortensen, and K. Yvind, "Effective electro-optical modulation with high extinction ratio by a graphene–silicon microring resonator," *Nano Lett.*, vol. 15, no. 7, pp. 4393–4400, Jun. 2015.

[21] S. Yu *et al.*, "All-optical graphene modulator based on optical Kerr phase shift," *Optica*, vol. 3, no. 5, pp. 541–544, May 2016.

[22] H. Dalir, Y. Xia, Y. Wang, and X. Zhang, "Athermal broadband graphene optical modulator with 35 GHz speed," *ACS Photon.*, vol. 3, no. 9, pp. 1564–1568, Sep. 2016.

[23] L. Abdollahi Shiramin and D. Van Thourhout, "Graphene modulators and switches integrated on silicon and silicon nitride waveguide," *IEEE J. Sel. Topics Quantum Electron.*, vol. 23, no. 1, pp. 94–100, Jan. 2017.

[24] A. Pitilakis, D. Chatzidimitriou, T. V. Yioultsis, and E. E. Kriezis, "Asymmetric Si-slot coupler with nonreciprocal response based on graphene saturable absorption," *IEEE J. Quantum Electron.*, vol. 57, no. 3, pp. 1–10, Jun. 2021.

[25] Y. Wang, C. Xue, Z. Zhang, H. Zheng, W. Zhang, and S. Yan, "Tunable optical analog to electromagnetically induced transparency in graphene-ring resonators system," *Sci. Rep.*, vol. 6, no. 1, Dec. 2016, Art. no. 38891.

[26] J. Kim, H. Son, D. J. Cho, B. Geng, W. Regan, S. Shi, K. Kim, A. Zettl, Y.-R. Shen, and F. Wang, "Electrical control of optical plasmon resonance with graphene," *Nano Lett.*, vol. 12, no. 11, pp. 5598–5602, Oct. 2012.

[27] V. P. Gusynin and S. G. Sharapov, "Transport of dirac quasiparticles in graphene: Hall and optical conductivities," *Phys. Rev. B, Condens. Matter*, vol. 73, no. 24, Jun. 2006, Art. no. 245411.

[28] G. W. Hanson, "Dyadic Green's functions and guided surface waves for a surface conductivity model of graphene," *J. Appl. Phys.*, vol. 103, no. 6, Mar. 2008, Art. no. 064302.

[29] Q. Bao and K. P. Loh, "Graphene photonics, plasmonics, and broadband optoelectronic devices," *ACS Nano*, vol. 6, no. 5, pp. 3677–3694, May 2012.
[30] M. Breusing, C. Ropers, and T. Elsaesser, "Ultrafast carrier dynamics in graphite," *Phys. Rev. Lett.*, vol. 102, no. 8, Feb. 2009, Art. no. 08680.
[31] Z. Sun, T. Hasan, F. Torrisi, D. Popa, G. Privitera, F. Wang, F. Bonaccorso, D. M. Basko, and A. C. Ferrari, "Graphene mode-locked ultrafast laser," *ACS Nano*, vol. 4, no. 2, pp. 803–810, Feb. 2010.
[32] D. Sun, Z.-K. Wu, C. Divin, X. Li, C. Berger, W. A. de Heer, P. N. First, and T. B. Norris, "Ultrafast relaxation of excited dirac fermions in epitaxial graphene using optical differential transmission spectroscopy," *Phys. Rev. Lett.*, vol. 101, no. 15, Oct. 2008, Art. no. 157402.
[33] P. A. George, J. Strait, J. Dawlaty, S. Shivaraman, M. Chandrashekhar, F. Rana, and M. G. Spencer, "Ultrafast optical-pump terahertz-probe spectroscopy of the carrier relaxation and recombination dynamics in epitaxial graphene," *Nano Lett.*, vol. 8, no. 12, pp. 4248–4251, Dec. 2008.
[34] R. Hao, W. Du, H. Chen, X. Jin, L. Yang, and E. Li, "Ultra-compact optical modulator by graphene induced electro-refraction effect," *Appl. Phys. Lett.*, vol. 103, no. 6, Aug. 2013, Art. no. 061116.
[35] Y. Hu, M. Pantouvaki, J. Van Campenhout, S. Brems, I. Asselberghs, C. Huyghebaert, P. Absil, and D. Van Thourhout, "Broadband 10 Gb/s operation of graphene electro-absorption modulator on silicon," *Laser Photon. Rev.*, vol. 10, no. 2, pp. 307–316, Mar. 2016.

YONGHUA WANG received the Ph.D. degree in instrument science and technology from the North University of China, in 2016. He is currently working as a Postdoctoral Research Fellow with the College of Physics and Optoelectronic Engineering, Shenzhen University. His present scientific interests include silicon photonics, nanoscale science and technology, including the nanofabrication, nonlinear optics, and nanomaterials.

LEI LEI received the Ph.D. degree from the Huazhong University of Science and Technology (HUST), Wuhan, China, in 2014. She completed part of her research at the Technical University of Denmark (DTU), as a Visiting Researcher Assistant, in 2013. From 2014 to 2015, she worked as a Postdoctoral Research Fellow with the Institute National de la Recherche Scientifique–Centre Energie, Matériaux et Télécommunications (INRS-EMT), Montreal, QC, Canada. She is currently an Associate Professor with the College of Physics and Optoelectronic Engineering, Shenzhen University. Her research interests include nanophotonics, high-speed optical communications, metamaterials, and plasmonics.

JUNBIN ZANG received the B.S. degree in computer science and technology and the M.S. degree in precision instrument and machinery from the North University of China, Taiyuan, China, where he is currently pursuing the Ph.D. degree in instruments and electronic engineering with the Key Laboratory of Instrumentation Science and Dynamic Measurement, Ministry of Education. His current research interest includes the design of the MEMS stethoscope.

WENCHAN DONG received the Ph.D. degree from the Huazhong University of Science and Technology (HUST), Wuhan, China, in 2018. She currently holds a postdoctoral position with the Wuhan National Laboratory for Optoelectronics, Institute of Optoelectronics Science and Engineering, HUST. Her current research interests include optical computing and signal processing based on integrated devices.

XINLIANG ZHANG (Senior Member, IEEE) received the Ph.D. degree in physical electronics from the Huazhong University of Science and Technology (HUST), Wuhan, China, in 2001. He is currently with the Wuhan National Laboratory for Optoelectronics, School of Optical and Electronic Information, HUST, as a Professor. He is the author or coauthor of more than 300 journal articles and conference papers. His current research interests include InP-based and Si-based devices, integration for optical networks, high-performance computing, and microwave photonics. In 2016, he was elected as an OSA Fellow.

PING XU received the Ph.D. degree from Sichuan University, Chengdu, China, in 1996. He is currently with the College of Physics and Optoelectronic Engineering, Shenzhen University, as a Professor. His current research interests include micro optics and binary optics, optical passive devices, and information optics.